CrossMark

Simulating seasonal tropical cyclone intensities at landfall along the South China coast

Charlie C. F. Lok[1] · Johnny C. L. Chan[1]

Abstract A numerical method is developed using a regional climate model (RegCM3) and the Weather Forecast and Research (WRF) model to predict seasonal tropical cyclone (TC) intensities at landfall for the South China region. In designing the model system, three sensitivity tests have been performed to identify the optimal choice of the RegCM3 model domain, WRF horizontal resolution and WRF physics packages. Driven from the National Centers for Environmental Prediction Climate Forecast System Reanalysis dataset, the model system can produce a reasonable distribution of TC intensities at landfall on a seasonal scale. Analyses of the model output suggest that the strength and extent of the subtropical ridge in the East China Sea are crucial to simulating TC landfalls in the Guangdong and Hainan provinces. This study demonstrates the potential for predicting TC intensities at landfall on a seasonal basis as well as projecting future climate changes using numerical models.

Keywords Tropical cyclone landfall · Tropical cyclone intensity · Downscaling · Regional climate model · WRF · East Asia

1 Introduction

Tropical cyclones (TCs) are one of the most powerful weather systems on Earth. An accurate TC forecast is important for protecting life and property, and hence scientists have been conducting extensive research for decades. The western North Pacific (WNP), with coastal areas being home to over a billion people, has, in general, the highest number of TCs of any ocean basin. Numerous studies have been carried out to understand the variability of TCs in this region. They are summarised in the following paragraphs.

Chan (1985) first addressed the interannual variability of TC activity in the WNP and its relationship with the El Niño-Southern Oscillation (ENSO). Variations in TC occurrence have been further investigated in later studies (e.g., Chan 2000; Wang and Chan 2002; Camargo and Sobel 2005; Ho et al. 2009). Many scientists have also examined possible effects of anthropogenic global warming on TC variability by analysing past observations and performing numerical simulations. Knutson et al. (2010) reviewed these studies in detail.

While these studies provided important knowledge on TC climatology in the WNP, fewer have investigated variations of TC landfall in East Asia and the possible causes of such variations specifically. Chan and Xu (2009) conducted an initial study and found interannual to multidecadal oscillations of TC landfall occurrence, but little is known about the variation in TC intensity. Recently, Liu and Chan (2017) examined TC landfall intensities using the annual power dissipation index (APDI), which sums the cube of the TC maximum sustained wind at landfall for all TCs that make landfall in a region of a year, and identified possible linkages between the regional APDI and the large-scale atmospheric environment. They proposed that active/inactive periods of the APDI in different regions can be linked to the cyclonic/anticyclonic phases of three anomalous circulation cells, which are located to the east of Japan, the east of Taiwan and in the northern South China Sea.

✉ Charlie C. F. Lok
   charlie.lok@my.cityu.edu.hk

[1] School of Energy and Environment, City University of Hong Kong, 83 Tat Chee Avenue, Kowloon Tong, Hong Kong

However, the physical mechanism behind such relationships is still unclear.

Recreating TC climatology using numerical models can help us understand these mechanisms and make predictions. Statistical approaches (e.g., Watterson et al. 1995; Lander 1996; Chan et al. 1998) have been used to relate large-scale forcing to future TC activity so that seasonal predictions can be made. With finer resolution models and increasing computational power, TCs have become resolvable in global or regional climate models (e.g., Vitart and Stockdale 2001; Knutson et al. 2007). It is thus possible to predict TC activity dynamically.

In the WNP, regional climate models have been employed to investigate dynamical interactions between the environment and TC activity. For example, Stowasser et al. (2007) analysed the response of TC activity to a warming climate using a global circulation model. Using the WRF climate model, Jin et al. (2012) found that off-equatorial sea surface temperature warming can lead to more TCs entering the northern part of East Asia.

In terms of seasonal variations, Au-Yeung and Chan (2012) tested the ability of a regional climate model to predict WNP TC activity. A follow-up study by Huang and Chan (2014) explored its potential in simulating TCs making landfall in three different East Asia regions. They further showed that the regional model can provide better regional TC landfall forecasts than the global model. Both studies demonstrated good potential in predicting regional TC landfalls on a seasonal basis. However, their works did not examine TC intensities at landfall.

In light of these previous observational and numerical studies, it is desirable to examine the ability of numerical models to predict TC intensities at landfall on a seasonal timescale. The objectives of this study are therefore: (a) to develop a numerical procedure capable of simulating the climatology of TC landfall intensities, which is first tested for TCs within the South China region; (b) to evaluate the simulation results and find the optimal model configurations; and (c) to identify the possible factors that are important to the model performance.

The numerical procedure of simulating the climatology of TC landfalls is presented in Sect. 2, and different model configurations are evaluated in Sect. 3. Section 4 examines the simulated TC landfall climatology, and the model predictability is discussed in Sect. 5. A summary is given in Sect. 6.

2 Model design

Two numerical models are used to simulate the seasonal variations of TC landfall frequency and intensity. A regional climate model is first run to simulate the atmospheric conditions throughout the main WNP TC season (from May to October). From the regional model outputs, TC-like vortices are identified and tracked until landfall. If a TC-like vortex makes landfall within the area of interest, a mesoscale model is run from the regional model outputs so that the vortex can be properly spun up. By nesting a higher resolution model, a better TC structure at landfall should be obtained. Details of the model design are further elaborated in the following sub-sections, and the model setup is evaluated in Sect. 3.

2.1 Regional climate model

The ICTP Regional Climate Model version 3 (hereafter RegCM3 Pal et al. 2007) is used in this study to produce seasonal simulations for the entire WNP. It is a compressible, sigma coordinate model, based on the hydrostatic dynamical core of the fifth-generation Pennsylvania State University-National Center for Atmospheric Research Mesoscale Model. Details of the model and the available physical packages are documented in Pal et al. (2007).

In this study, physical schemes are employed according to the investigations of Au-Yeung and Chan (2012) and Huang and Chan (2014). The model uses the modified Biosphere-Atmosphere Transfer Scheme for the land surface processes (Dickinson et al. 1986), the Holtslag et al. (1990) boundary layer scheme and the radiative transfer scheme of the NCAR Community Climate Model version 3 (Kiehl et al. 1996). A subgrid explicit moisture scheme (Pal et al. 2000) is used for the model-resolvable, non-convective precipitation. For cumulus convection, Huang et al. (2013) found that the MIT scheme (Emanuel and Živković Rothman 1999) with the modifications suggested by Chow et al. (2006) was the best scheme in simulating East Asia summer rainfall and so this scheme is also used in our WNP TC simulations. Chow et al. (2006) found that the original MIT scheme overestimated the East Asia summer precipitation, and proposed two large-scale criteria to reduce such bias. The same modifications are applied to RegCM3 in this study, in which convective precipitation is prohibited if the relative humidity is less than 55%, or the low-level flow is anticyclonic with the absolute magnitude of the relative vorticity exceeding 12×10^{-6} s^{-1}.

The NCEP Climate Forecast System reanalysis data (CFSR, Saha et al. 2010) are used as the atmospheric initial and lateral boundary conditions and also for the underlying sea surface temperature. Huang and Chan (2014) reported that the CFSR dataset is more suitable for regional TC simulation than the ERA 40 reanalysis (Uppala et al., 2005), which was used by Au-Yeung and Chan (2012). It should be noted that Huang and Chan (2014) also used the real-time CFS2 re-forecast outputs (Saha et al. 2014) to simulate TC landfalls after 2000, and it would be desirable for us to

use the same dataset. However, those 6-hourly 9-month re-forecast outputs are no longer available, and consequently in this study our model is driven entirely by the CFSR.

The CFSR boundary conditions are fed into RegCM3 every 6 h via a 15-grid buffer relaxation method, and sea surface temperature is updated weekly. The model contains 18 vertical levels from the surface up to 1 hPa. The horizontal domain extends from 90°E to 170°W and 15°S to 45°N, with 50 km grid spacing. The RegCM3 domain is shown as a solid grey box in Fig. 1. The period between 1990 and 2010 is investigated. For each year, the RegCM3 simulation starts in early April and runs until the end of October. In order to estimate the uncertainty of the RegCM3 model, eight ensemble runs are performed by separating the model starting time every 6 h. The first ensemble member starts at 1 April 00Z and the last one at 2 April 18Z every season. Au-Yeung and Chan (2012) showed that the use of an 8-member ensemble is enough to capture most of the model uncertainty. The first month of the simulation (i.e. April) is regarded as the model spin-up period, and only the outputs between May and October are used.

2.2 Tracking TC landfalls in RegCM3

A TC tracker similar to the one used in Au-Yeung and Chan (2012) and Huang and Chan (2014) is used to trace vortices with TC characteristics from the RegCM3 outputs. The tracker first identifies all local 850-hPa vorticity maxima within a 10° latitude square box, and a TC is declared if: (a) the maximum vorticity is greater than 450×10^{-6} s^{-1} (negative in Southern Hemisphere); (b) 300-hPa air temperature at the vortex centre is 1 K warmer than the mean value within a 15° latitude square box from the vortex centre; (c) the vortex has met criteria (a) and (b) for at least 48 h consecutively; and (d) the genesis position is over the ocean.

A TC-like vortex is regarded as making landfall at a certain region if its centre is less than 100 km from the coastline, following the practice of Liu and Chan (2017). Due to limited computational power, only the vortices making landfall in the Guangdong and Hainan provinces (the area bounded by the solid black line in Fig. 1, hereafter South China) will be further simulated by a mesoscale model in this study.

2.3 Mesoscale model

For every RegCM3 vortex identified as making landfall in South China, the Weather Research and Forecast model version 3.7 (hereafter WRF) is nested on the RegCM3 outputs in order to obtain the detailed TC structure as well as its intensity at landfall. The WRF is a compressible, non-hydrostatic Eulerian model (Skamarock et al. 2008). It is widely used in numerical studies with numerous options for different situations, and the model configuration used in this study is briefly described in the following paragraphs.

The model contains two domains (outer and inner) with horizontal resolutions of 27 km (151×151 grid points) and 9 km (181×181 grid points). To allow sufficient time for the vortex to spin up, the WRF model starts 60 h prior to the RegCM vortex landfall. The outer domain is centred at the RegCM vortex position 30 h prior to the landfall, and the inner domain is initially centred at the vortex position 60 h before the landfall. The two domains exchange information bidirectionally at every timestep (two-way grid nesting), and a vortex tracing algorithm based on 500-hPa relative vorticity is applied to keep the vortex within the inner domain. As such, the inner domain is relocated every 15 model minutes. The WRF model consists of 28 vertical levels from the surface up to 100 hPa. The timestep ratio of the outer and inner domain is 1:3, the same as the horizontal grid spacing ratio.

The physical packages of the WRF model chosen in this study are: the Ferrier et al. (2002) schemes for microphysics, the Yonsei University scheme (Hong et al. 2006) for the planetary boundary layer, the Kain (2004) scheme for cumulus convection, the Rapid Radiative Transfer Model (Mlawer et al. 1997) for radiation and the MM5 similarity scheme based on Monin and Obukhov (1954) for the surface layer. Due to the lack of soil temperatures in the RegCM3 outputs, the 5-layer thermal diffusion is the only available choice for the land surface model.

Based on the WRF simulations of all landfalling vortices, a comprehensive set of TC landfalls can be obtained. The simulations are validated against the Joint Typhoon Warning Center (JTWC) best track dataset (Chu et al. 2002), which contains all of the actual TC landfalls and intensity estimates at landfall.

3 Model sensitivity tests

Since there are many different model configurations to choose from, it is important to verify whether the setting described in Sect. 2 is indeed the optimal one for simulating TCs making landfall in the South China region. Three sensitivity tests are therefore designed, and each test offers an alternative choice of: RegCM3 domain (Experiment 1), WRF horizontal resolution (Experiment 2) and WRF physical packages (Experiment 3). By comparing the simulated TC landfalls with the new setting against the result from the default setting (hereafter the default), the most suitable model setup can be determined. Configurations of the three sensitivity experiments and the default are shown in Table 1.

Table 1 Model configurations altered in the sensitivity tests as presented in Sect. 3

Simulation	Model	Years	Resolution	RegCM3 longitude	WRF microphysics	Cumulus
Default	RegCM	1990–2010	50 km	90°E–170°W		Modified MIT scheme
	WRF		27, 9 km		Ferrier et al. (2002)	Kain (2004)
Experiment 1	RegCM	2001–2010	50 km	74°E–172°W		Modified MIT scheme
Experiment 2	WRF	1998, 2000, 2003, 2010	18, 6 km	90°E–170°W	Ferrier et al. (2002)	Kain (2004)
Experiment 3	WRF	1998, 2000, 2003, 2010	27, 9 km	90°E–170°W	WSM-6	Tiedtke (1989)

The default row represents parts of the model setup described in Sect. 2 to be compared against sensitivity experiments. Experiment 1 tests the sensitivity of the RegCM3 domain and does not include the WRF simulation. For Experiments 2 and 3, all WRF simulations are nested on the same RegCM3 outputs using the default setting to examine the TC intensity dependencies on the WRF configuration
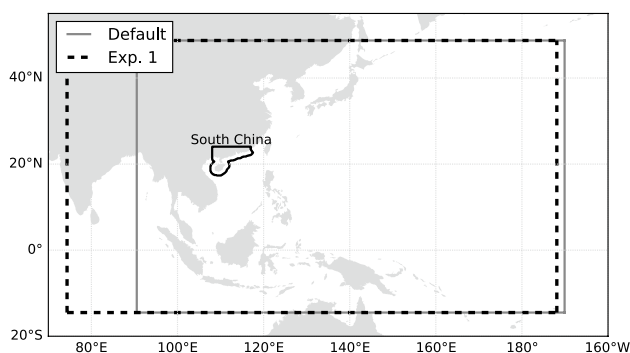

Fig. 1 Map of the RegCM3 simulation domains and the area of interest. The *grey solid box* represents the area of coverage in the "default" setting whereas the *black dashed box* is used for Experiment 1. The *black solid line* is the boundary of the area of interest in this study (South China). Any TC entering this area is considered as making landfall in South China

Fig. 2 Annual number of TC landfalls in South China between May to October. *Grey bars* are the observed numbers from the JTWC best track, with a minimum TC intensity of 35 knots; *squares* represent the ensemble means from the default simulation, with *thick whiskers* showing the spreads between ensemble members. *Solid circles* are the ensemble means from the Experiment 1 run, with *thin whiskers* for the ensemble spreads

3.1 Experiment 1: RegCM3 domain

This experiment tests whether RegCM3 better simulates the number of TC landfalls if the entire Tibetan Plateau is part of the domain. As regional climate models often run for at least several months, regional processes are important in simulating weather events. Prior research has suggested that the regional model could be sensitive to the choice of domain, but the dependency varies case by case (e.g., Bhaskaran et al. 2012; Landman et al. 2005). For simulating summertime events in East Asia, Huang et al. (2013) reported that RegCM3 produced a more accurate precipitation distribution when the domain covered the entire Plateau. Following Huang et al. (2013)'s finding, the western boundary of Experiment 1 is set at 75°E (the dashed black box in Fig. 1), which is different from the default's west end of 90°E.

The result of this experiment, however, does not suggest significant dependence on the model domain. Both simulations have similar predictions throughout the period from 2001 to 2010, as shown in Fig. 2. While Experiment 1 has a smaller root mean square error (1.74 TC landfalls per year)
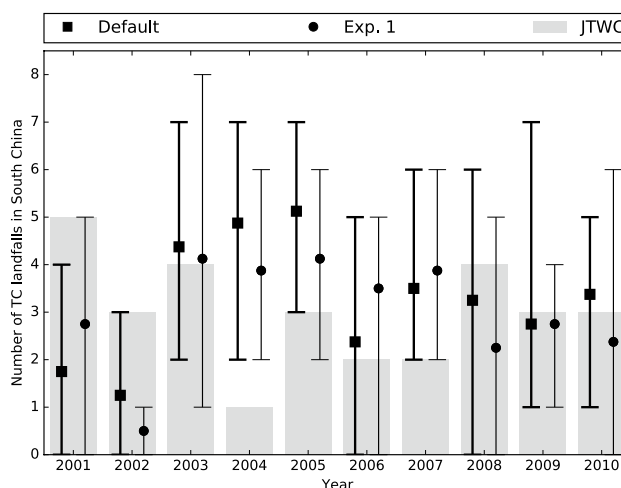
than the default's error of 1.90, it should be noted that the difference is mostly contributed by the deficit in 2004. Only two TCs entered the northern South China Sea between May and October 2004, and only one of them eventually made landfall. It is only the second time that such a lull occurred since the satellite era began in 1979. In fact, neither simulation could reproduce the low activity in the South China Sea in 2004. If a less outlier-penalising metric, such as mean absolute error is used, both Experiment 1 and the default have the same error score of 1.55.

A paired t test is also conducted to determine if the seasonal ensemble means of TC landfalls using the two configurations are significantly different. Among the 10 investigated seasons, the smallest p value is only 0.14, which means any difference in the two ensemble means is at most significant at 86% confidence level only. In fact, the p values are smaller than 0.20 in just two seasons, and for the

other five seasons the p values are even higher than 0.25. In other words, the difference between the default and Experiment 1 in terms of seasonal TC landfalls is not significant. Hence, it can be concluded that RegCM3 is not sensitive to the inclusion of the Tibetan Plateau in predicting the number of TC landfalls in South China.

3.2 Experiment 2: WRF horizontal resolution

The sensitivity of TC intensity and structure to the mesoscale model resolution has been well documented (e.g., Fierro et al. 2009; Gentry and Lackmann 2010; Jin et al. 2014). They found that with higher resolution, models can generate more realistic convection and in return better simulate TC intensification. Given that the focus of this study is on the TC intensity at landfall, it is important to check if such sensitivity also exists.

In the second sensitivity experiment, the horizontal resolutions of the WRF's outer and inner domains are increased to 18 and 6 km respectively, whereas the default setting is 27 and 9 km. Based on the same RegCM3 simulated TC landfall with the default RegCM3 configuration, the effect of the resolution on TC intensity simulation is examined. It should be noted that although it would be desirable to further increase the resolution, 6 km is the highest horizontal resolution our computers are capable of running. The sensitivity experiment resimulates RegCM3 TC landfalls in four seasons (1998, 2000, 2003 and 2010) and compares the results with those from the default. The choice of years is intended to be representative of the overall RegCM3 performance. For 2003 and 2010, RegCM3 accurately predicts the number of TC landfalls while it does not accurately predict landfalls in 1998 and 2000 (see Fig. 8).

Figure 3 shows the WRF-simulated intensity distributions from the default and Experiment 2. Despite having finer grid spacing, the simulated peak intensity distribution from Experiment 2 only shifts slightly to a stronger regime. In fact, TCs from the higher resolution run are only 3.45 knots stronger at their peak, and the difference is reduced to 1.65 knots at the time of TCs making landfall. While the intensity differences are significant at the 99% confidence level, the impact of a finer horizontal resolution on TC intensities at landfall is apparently small.

In order to examine the seasonal variations of TC intensities at landfall, Liu and Chan (2017) used the annual power dissipation index (APDI) to include both the number of TCs making landfall and their intensities at landfall. The index is the sum of the cube of the maximum sustained wind speed at landfall of each TC making landfall in a particular region, which in this study is the South China coast.

The observed average APDI among the selected years is 10.5×10^5 knots^3, while the default and Experiment 2 predict 14.2 and 15.3×10^5 knots^3 respectively. The
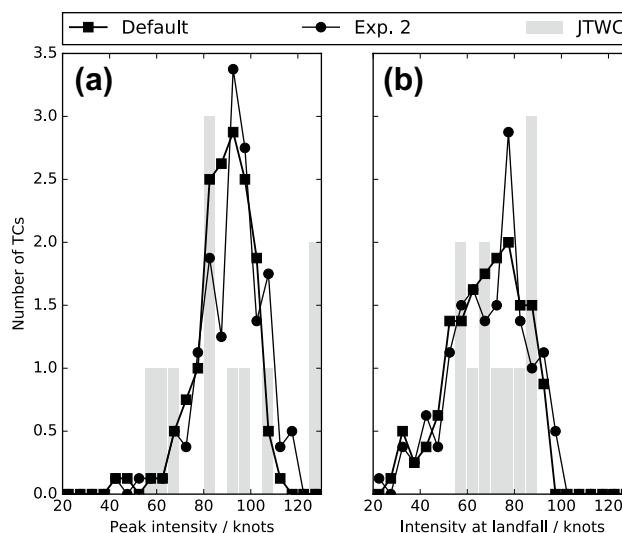

Fig. 3 Distributions of simulated TC maximum sustained wind at: **a** peak intensity within 60 h prior to landfall and **b** at landfall. The default simulation is shown in *thick squared lines* and Experiment 2 in *thin solid circle* lines. The *grey bar* is the distribution of the JTWC best track

root mean square error of the APDI for the default run is 6.7×10^5 knots^3, which is 1.0×10^5 knots^3 smaller than the RMSE of Experiment 2 (7.7×10^5 knots^3). In terms of individual seasons, the default is also superior in all four selected years (not shown). It is clear that the default WRF resolution is a better choice in this case. Since the WRF model used in this study has no ocean coupling, such overestimation might be expected (Gentry and Lackmann 2010). Furthermore, as will be shown in the next section, the WRF model in fact tends to overpredict TC intensity at landfall. Adopting a higher resolution in this study will further enhance the undesirable bias. As a result, the alternative of using higher model resolution should not be applied.

3.3 Experiment 3: WRF physical options

Various physical packages in the WRF model have different convection characteristics. Such model sensitivity has been investigated (e.g., Gallus and Bresch 2006; Hong et al. 2009), and TC structure and intensity are no exception. Parker et al. (2013) examined a few combinations of physical schemes and documented their performances for Cyclone Yasi (2011). Although they found an optimal selection for their particular case, they noted that their finding is not universal, and further investigation is required for other scenarios. The third sensitivity test is therefore to determine which of the two combinations has better skill: the WSM-6 scheme (Hong and Lim 2006) combined with the Tiedtke (1989) scheme, suggested by the model developers for TC simulation (Skamarock et al., 2008); or the

Ferrier et al. (2002) and the Kain (2004) schemes (default), deemed optimal for reproducing the intensity of Cyclone Yasi (Parker et al. 2013).

With the new physical combination, simulated TCs are slightly weaker than the default (Fig. 4). The shift of intensity distribution however is once again small, and this time the difference in mean landfall intensity is not significant. Two simulated intensity distributions have 83% area overlap, and both simulations capture 66% of the observed distribution. Also, the root mean square error of the APDI simulated by Experiment 3 is the same as the default (6.7×10^5 knots^3). Since the runs are similar to each other, it can be concluded that the model is not sensitive to the choice of physical packages in simulating TC intensities at landfall seasonally.

In summary, none of the above three sensitivity tests demonstrate better model skill with an alternative configuration. The model either has no dependence on that particular setting, or the default setting performs better than the new one. As such, the default setting is adopted to simulate TC landfalls for the rest of this study.

4 Simulated TC landfall climatology between 1990 and 2010

The TC climatology from 1990 to 2010 is reproduced using the model setup described in Sect. 2. In general, the simulated and the observed WNP TC distributions are similar to each other, as shown in Fig. 5. The spatial correlation coefficient between the projected and observed frequencies has a value of 0.96 which is significant at the 95%
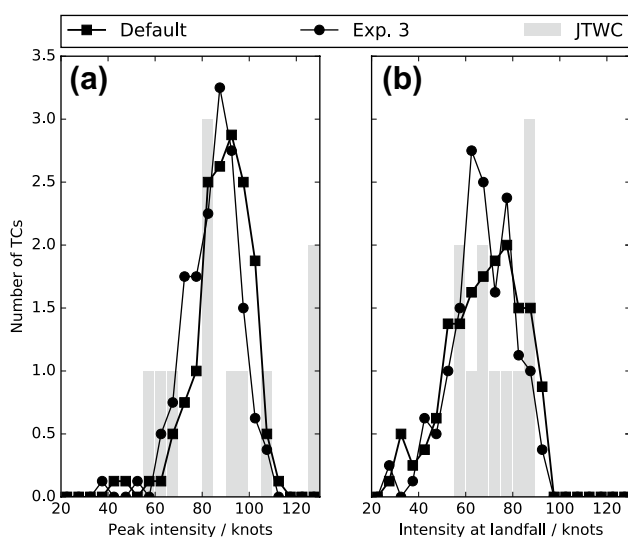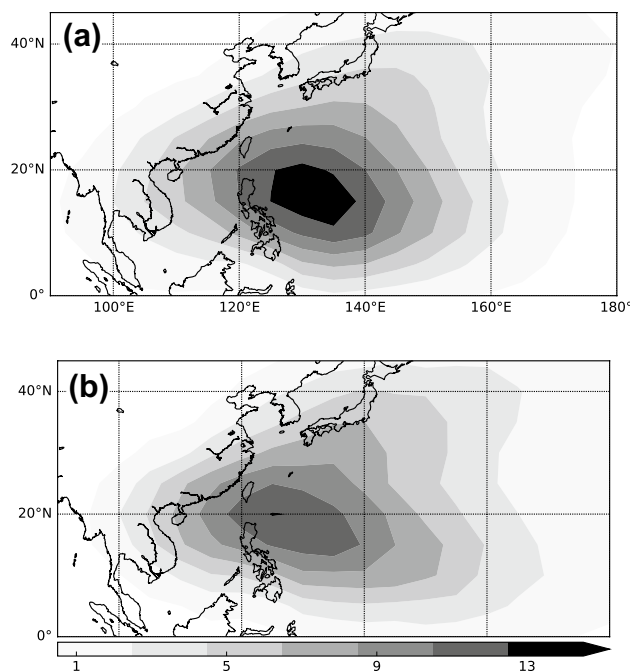

Fig. 5 Distribution of the May–October TC activity in the western North Pacific between 1990 and 2010 from **a** the RegCM3 ensemble means and **b** the JTWC best tracks. Unit is number of TC passages per 5° × 5° square per year

confidence level. This reaffirms RegCM3's ability in recreating the current TC climatology, and is in agreement with Au-Yeung and Chan (2012). However, a noticeable difference is found once the simulated distribution is subtracted from the best track in Fig. 6. The simulation contains a southward bias: overpredicting the number of TCs at lower latitudes, in particular to the east of the Philippines and underpredicting the number of TCs in the northern part of the domain. The bias is likely due to an overestimation of the WNP subtropical high in RegCM3. Nevertheless, the error of TC passages in coastal South China is only about
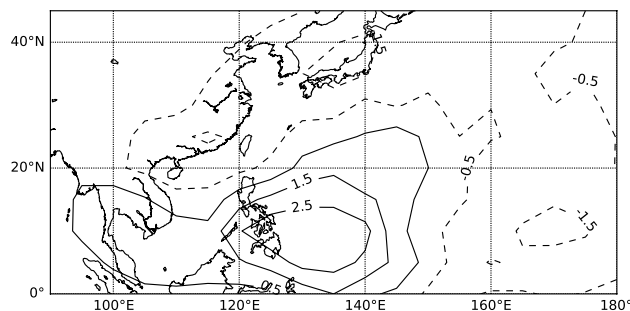

Fig. 4 Same as Fig. 3 except the *thin solid circle lines* represent the results from Experiment 3

Fig. 6 The difference between the RegCM3 simulated and observed May to October TC activity in the western North Pacific between 1990 and 2010. Contoured every 1 TC passages per 5° × 5° *square box* per year. *Solid* (*dashed*) *lines* represent overprediction (underprediction)
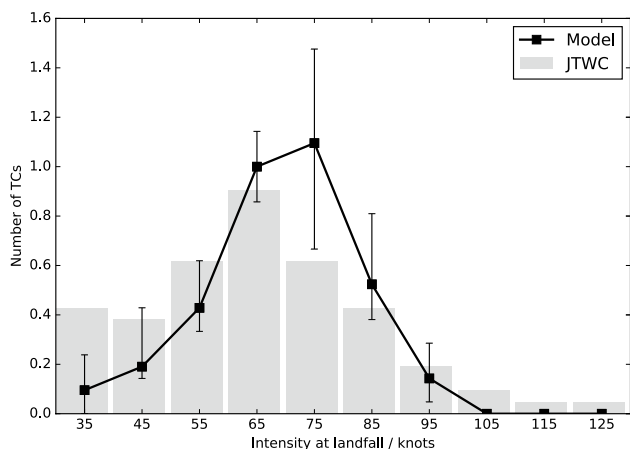
Fig. 7 Intensity distribution of the TCs making landfall in South China from 1990 to 2010. *Grey bars* are the JTWC data. *Squared line* plots the model result with whiskers showing the ensemble spreads. TC intensities are grouped every 10 knots, and the median values are shown. TCs with maximum sustained winds less than 30 knots are excluded
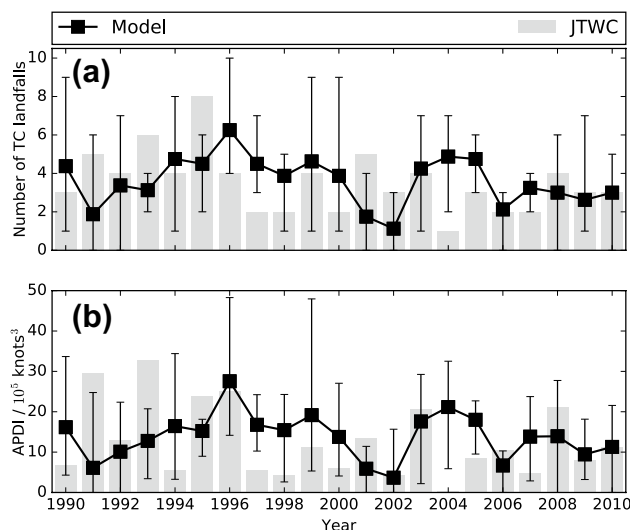

Fig. 8 Time series of **a** annual numbers of TC landfalls and **b** the APDI in South China between May and October. *Grey bars* are the observed values from the JTWC best track, with minimum TC intensity of 35 knots; *squares* represent the ensemble means from the simulation, with *whiskers* showing the spreads between ensemble members

1 TC per year. The result reaffirms the model's potential in simulating TC landfalls in the region, as reported in Huang and Chan (2014).

The RegCM3-WRF model system also demonstrates skill in recreating the climatology of TC intensity at landfall. The simulated distribution of TC intensity at landfall is similar to the observed distribution over the two decades studied here (Fig. 7). The correlation is about 0.78 which

is significant at the 95% confidence level, implying that a realistic TC intensity distribution at landfall can be reproduced by dynamical downscaling. It should be noted that the TC tracer presented in Sect. 2 is tuned for named TCs, i.e. maximum sustained winds of 34 knots or above. As such, the tracker will discard weak TC-like vortices, and it can be expected that the model system will underestimate the number of weak TCs (45 knots or below in Fig. 7).

Huang and Chan (2014) showed that RegCM3 is capable of predicting the annual number of TC landfalls in the "southern group" of East Asia, which includes South China, Vietnam and the Philippines. In this study, model performance for both the number of TC landfalls and their intensities at landfall in South China is examined. The root mean square error (RMSE) of the number of TC landfalls is 2.07, which is only 3% larger than the RMSE of the "southern group" reported in Huang and Chan (2014). Also, the RMSE of the simulated APDI is found to be 10.6×10^5 knots[3], which is 15% smaller than the RMSE from the CFSR, even though it is a reanalysis dataset instead of a forecast product. Furthermore, Fig. 8 shows that both the observed seasonal TC landfalls and their intensities in South China are within the model ensemble spread for most seasons. The comparison above suggests that the model system is capable of recreating a realistic TC landfall climatology.

To further assess the ensemble component of the model system, the rank histogram (Anderson 1996) is used. Hamill (2001) explained the interpretation of the histogram in detail. Its application in this study is summarised as follows. For each individual season, the simulated number of TC landfalls and APDI from every ensemble member are sorted from lowest to highest, and the corresponding observations are ranked relative to the sorted data. For example, the observed landfall number/APDI is ranked first if it is smaller than every ensemble member predicted number/APDI, and if the observation is larger than all members, the last rank (i.e. the number of ensembles plus one) is given. The rank histogram is plotted by tallying the ranks of all seasons. A flat histogram indicates a perfectly reliable simulation, and any departure from such uniformity can be seen as a model deficit.

The histograms for the number of TC landfalls and the APDI are shown in Fig. 9. Among the 21 simulated seasons, the model system is more likely to overestimate the number of TC landfalls, since the JTWC best track is ranked the first in 29% of the seasons. Also, for only 38% of the seasons the observations are ranked above median (the fifth rank). Such result suggests that the ensemble model appears to overestimate the number of TC landfalls. On the other hand, the histogram for the APDI (Fig. 9b) shows that while the observed APDI is ranked last in 24% of the seasons, the number of seasons ranked below the midpoint is
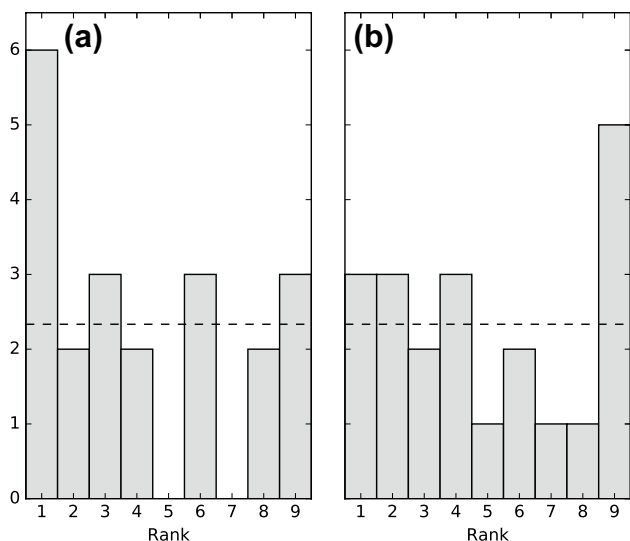
Fig. 9 Rank histograms for **a** the number of TC landfalls; **b** the APDI in South China. *Dashed lines* represent a idealised perfect ensemble model

Fig. 10 Correlation coefficients between RegCM3 seasonal mean 500 hPa geopotential height and the APDI in South China simulated by WRF. Correlations at 95% significance level or above are *shaded*

just 2 more than the seasons ranked above, which suggests that the model system is in fact able to recreate the variance of the APDI seasonally.

As departure from a uniform histogram (dashed lines in the Fig. 9) is regarded as a deficit of the ensemble, such departure can be measured by summing the absolute errors of each rank. It is found that the departure for the APDI is smaller than the number of TC landfalls, indicating that the ensemble system captures the variation of the TC intensities at landfall better than the number of landfalls alone.

The above analyses show that the model system is capable of recreating the climatology of TC landfalls. They also prove the system's ability to improve seasonal forecasts from a global model. Further adjustments are required, however, before the forecast of a particular region can be operationally produced.

5 Predictability of TC intensities at landfall

As the model system displays some skill in predicting TC landfalls and intensities in the South China region, it is also important to identify the reasons for such forecasts. This may help us understand the model behaviour and thus may potentially improve the system.

Correlation analysis is conducted for the May–October averaged 500-hPa geopotential height and the APDI in South China (Fig. 10). Significant positive correlations between these two variables can be found over Eastern China, with the peak correlation of 0.45 exceeding the 95% significance level. Also, at 850 hPa, a strong linkage
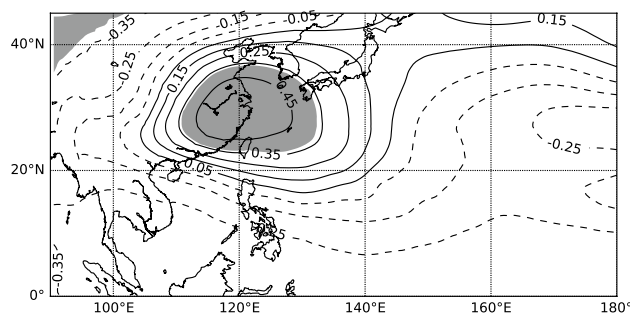
between TC landfalls and easterly (westerly) wind at 20°N (40°N) can also be seen from the model (Fig. 11). These two relationships together illustrate the influence of the subtropical high in the simulation of TC landfalls in South China. If the subtropical high extends westward, low-latitude easterlies are enhanced. As a result, more TCs are steered towards Guangdong. A similar relationship is also found between the actual APDI and reanalysis data (not shown). Such findings are consistent with the known cause of TC movement in the WNP (Chan and Gray 1982).

To further investigate how the large-scale environment affects the APDI in the model system, RegCM3 850–300 hPa layer-mean flow anomalies are composited for the highest and lowest 5 APDI years, which are the fourth and first quartiles respectively. Consistent with the correlation analysis, Fig. 12 shows dominant flow patterns centred over the East China Sea and covering most of the China coastline. During the quiet TC years simulated by the model system, there is abnormal southeastward flow in the northern South China Sea due to an enhanced cyclonic circulation centred on the East China Sea. The additional westerlies inhibit TCs entering the northern South China Sea and thus fewer make landfall (Fig. 12a). In the active years, on the other hand, the circulation over eastern China
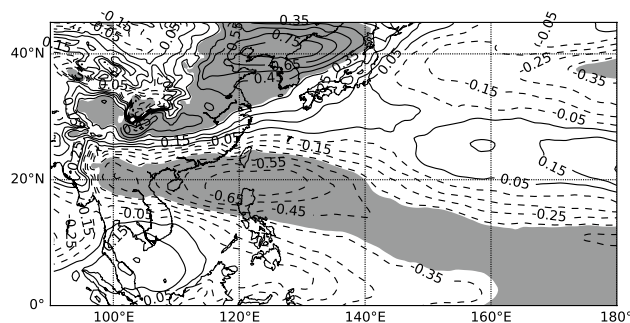

Fig. 11 As in Fig. 10 except for 850-hPa zonal winds. Noted that the positive (negative) values indicate correlation with west (east) wind
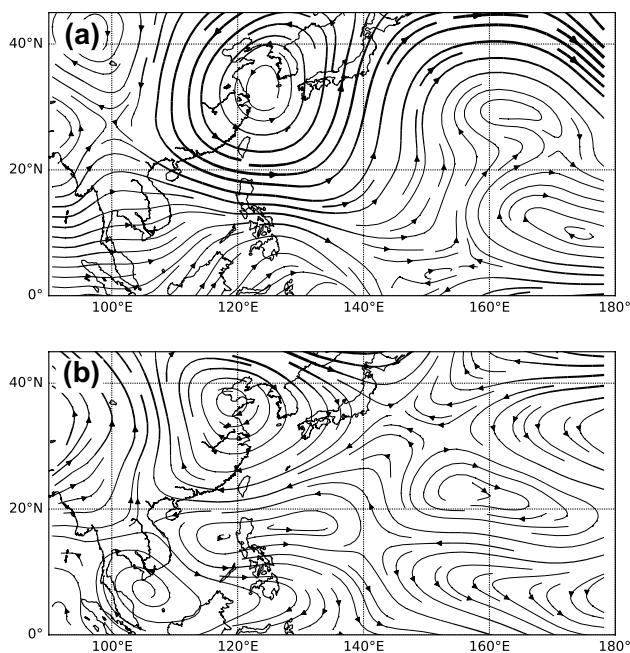
Fig. 12 Composites of the RegCM3 850–300 hPa layer-mean flow pattern anomalies of **a** the first quartile, **b** fourth quartile of annual TC landfalls in South China. The width of streamlines is proportional to wind speed

Fig. 13 Composites of RegCM3 500-hPa geopotential height one day prior to the WRF simulated TC landfalls, with TC intensities at landfall of **a** 25 m/s or below **b** 45 m/s or above. Units in metres

is anticyclonic, steering more TCs further west near 20°N (Fig. 12b). Additionally, low latitude westerlies can also be found in active years, leading to enhanced TC activity over the South China Sea. Similar patterns can also be found for the bottom and top quartiles of the number of TC landfalls in South China as well (not shown). These findings indicate that the characteristics of seasonal TC landfalls can be explained by the steering flow pattern over the WNP, as proposed in Liu and Chan (2017).

How the WRF model simulates individual TC intensity is also investigated. Composites of RegCM3 variables are produced according to the WRF-generated TC intensities. Since the RegCM3 outputs serve as initial and boundary conditions of WRF simulations, and the intensities of the corresponding RegCM3 vortices are not well correlated against the WRF simulated TC intensities, these composites help elucidate the reasons as to why the TC spins up in the WRF model. Figure 13a shows the composite RegCM3 500-hPa geopotential height pattern one day prior to TC landfall for the weakest 10% of TCs at landfall (i.e. 49 knots or below) and Fig. 13b for the strongest 10% (87 knots or above). In agreement with the seasonal TC landfalls, the location of the subtropical high is significantly different. For intense TC landfalls predicted by the WRF, the subtropical ridge during the previous 24 h is stronger, centred along the East China
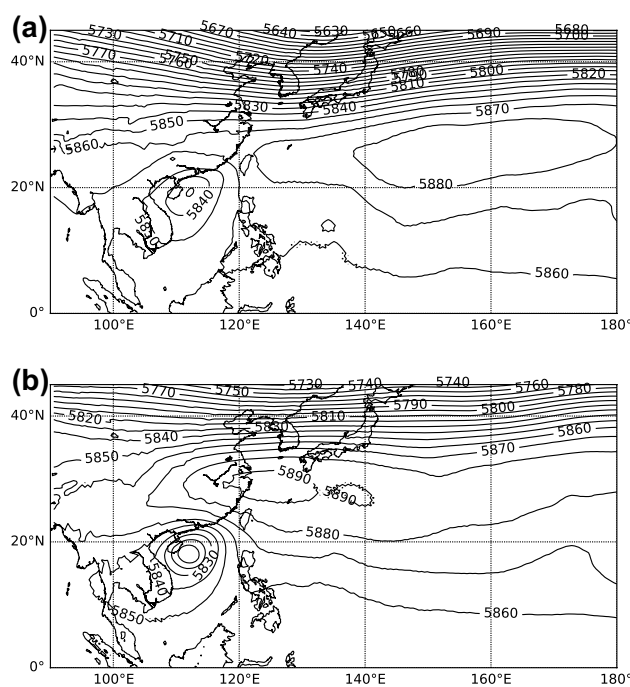
Sea and has its western edge extending up to 115°E (Fig. 13b). In contrast, during weak TC landfalls, the subtropical high remains in the middle of the WNP, far away from the TCs.

Not only does the subtropical ridge play an important role, the upper-level easterlies can also provide a favourable environment for TCs in the South China Sea. During strong TC landfalls, stronger 200-hPa easterlies are found at low latitudes along the South China Sea, where the TCs are located (Fig. 14b). This feature leads to the enhancement of an upper-level divergence in the northern South China Sea (shaded area), which can enhance TC outflows and further intensification. In contrast, for weak TCs, the large-scale circulation over the South China region is relatively weak, and upper level flow in the northern South China Sea is minimal. It is worth noting that the upper easterlies in the central South China Sea are not correlated with the subtropical high in the East China Sea. These findings share some similarity to the known interaction between upper-level flow, in particular tropical easterlies, and TC intensification (e.g., Davidson and Kar 2002; Wang and Wu 2016; Qian et al. 2016).

The above analyses suggest that, as long as the large-scale environment, in particular the subtropical high in WNP, can be accurately reproduced, seasonal TC landfalls and their intensities can also be predicted.
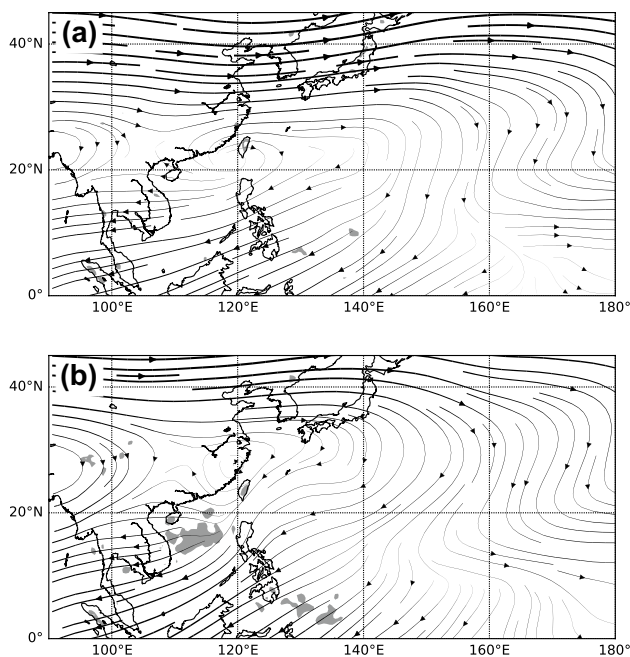
Fig. 14 Same as Fig. 13 but for 200-hPa streamlines. Streamlines width is proportional to wind speed and divergence larger than 15×10^{-6} s^{-1} is *shaded*

6 Summary

In this study, a numerical modelling system using both a regional climate model (RegCM3) and a mesoscale model (WRF) has been set up to simulate the number of TCs making landfall in South China, as well as their intensities at landfall. The model configurations have undergone three sensitivity tests on the choices of the RegCM3 model domain, the WRF horizontal resolution and the physical packages. Although none of the experimental runs has produced a better TC landfall climatology, such that the "default" setting is used, the finding is likely to be limited to this specific study, and extensive tests are still required for other applications, as have been pointed out in other sensitivity tests (e.g, Bhaskaran et al. 2012; Parker et al. 2013).

This study has found that the model system can reproduce a realistic TC landfall climatology in South China. The model skill in predicting the number of TCs making landfall in South China is comparable to Huang and Chan (2014), while it has been shown that the model system is able to capture the variations in seasonal TC intensity at landfall better than the number of landfalls alone. More importantly, it has been demonstrated that the model system can offer a better forecast of the seasonal intensity than a global model. The results indicate that the use of dynamic downscaling may provide useful seasonal predictions of TC intensities. However, further improvements of the model

skill and extensive tests with forecast data driving the regional model are necessary if the model system is to be used operationally.

The large-scale environment has also been shown to play a very important role on seasonal TC landfall frequency. If the subtropical high is strong over the East China Sea, TCs making landfall in South China tend to be stronger as well. In order to accurately predict the number of TC landfalls as well as their intensities on a seasonal basis, it is essential to have the subtropical ridge properly simulated.

Since the model system has demonstrated skill in simulating the climatology of the TC landfalls and intensities, and the model predictability is also identified, it is possible to use the model to simulate future climatology of TC intensities at landfall using the Coupled Model Intercomparison Project model outputs. The projection of the number and intensities of TC making landfall for the rest of this century in the region will be reported in the near future.

References

Anderson JL (1996) A method for producing and evaluating probabilistic forecasts from ensemble model integrations. J Clim 9(7):1518–1530

Au-Yeung AYM, Chan JCL (2012) Potential use of a regional climate model in seasonal tropical cyclone activity predictions in the Western North Pacific. Clim Dyn 39(3–4):783–794

Bhaskaran B, Ramachandran A, Jones R, Moufouma-Okia W (2012) Regional climate model applications on sub-regional scales over the indian monsoon region: the role of domain size on downscaling uncertainty. J Geophys Res D117(10):D10,113

Camargo SJ, Sobel AH (2005) Western North Pacific tropical cyclone intensity and ENSO. J Clim 18(15):2996–3006

Chan JCL (1985) Tropical cyclone activity in the Northwest Pacific in relation to the El Niño/Southern Oscillation phenomenon. Mon Weather Rev 113(4):599–606

Chan JCL (2000) Tropical cyclone activity over the Western North Pacific associated with El Niño and La Niña events. J Clim 13(16):2960–2972

Chan JCL, Gray WM (1982) Tropical cyclone movement and surrounding flow relationships. Mon Weather Rev 110(10):1354–1374

Chan JCL, Xu M (2009) Inter-annual and inter-decadal variations of landfalling tropical cyclones in East Asia. Part I: time series analysis. Int J Climatol 29(9):1285–1293

Chan JCL, Shi JE, Lam CM (1998) Seasonal forecasting of tropical cyclone activity over the Western North Pacific and the South China Sea. Weather Forecast 13(4):997–1004

Chow KC, Chan JCL, Pal JS, Giorgi F (2006) Convection suppression criteria applied to the MIT cumulus parameterization scheme for simulating the Asian summer monsoon. Geophys Res Lett 33(24):L24,709

Chu JH, Sampson CR, Levine AS, Edward F (2002) The Joint Typhoon Warning Center tropical cyclone best-tracks, 1945–2000. Report, Joint Typhoon Warning Center, Pearl Harbor (United States). http://www.usno.navy.mil/NOOC/nmfc-ph/RSS/jtwc/best_tracks/TC_bt_report.html. Accessed 15 July 2016

Davidson NE, Kar SK (2002) Upper-tropospheric flow transitions during rapid tropical cyclone intensification. Q J R Meteorol Soc 128(581):861–891

Dickinson RE, Henderson-Sellers A, Kennedy PJ, Wilson MF (1986) Biosphere-atmosphere transfer scheme (BATS) for the NCAR Community Climate Model. Technical Note TN-275+STR, National Center for Atmospheric Research, Boulder, Colorado (United States). https://opensky.ucar.edu/islandora/object/technotes:383/datastream/PDF/view. Accessed 15 July 2016

Emanuel KA, Živković Rothman M (1999) Development and evaluation of a convection scheme for use in climate models. J Atmos Sci 56(11):1766–1782

Ferrier BS, Jin Y, Lin Y, Black T, Rogers E, DiMego G (2002) Implementation of a new grid-scale cloud and precipitation scheme in the NCEP eta model. In: 19th conference on weather analysis and forecasting/15th conference on numerical weather prediction, American Meteorology Society, San Antonio (United States)

Fierro AO, Rogers RF, Marks FD, Nolan DS (2009) The impact of horizontal grid spacing on the microphysical and kinematic structures of strong tropical cyclones simulated with the wrf-arw model. Mon Weather Rev 137(11):3717–3743

Gallus WA, Bresch JF (2006) Comparison of impacts of WRF dynamic core, physics package, and initial conditions on warm season rainfall forecasts. Mon Weather Rev 134(9):2632–2641

Gentry MS, Lackmann GM (2010) Sensitivity of simulated tropical cyclone structure and intensity to horizontal resolution. Mon Weather Rev 138(3):688–704

Hamill TM (2001) Interpretation of rank histograms for verifying ensemble forecasts. Mon Weather Rev 129(3):550–560

Ho CH, Kim HS, Jeong JH, Son SW (2009) Influence of stratospheric quasi-biennial oscillation on tropical cyclone tracks in the Western North Pacific. Geophys Res Lett 36(6):L06,702

Holtslag AAM, de Bruijn EIF, Pan HL (1990) A high resolution air mass transformation model for short-range weather forecasting. Mon Weather Rev 118(8):1561–1575

Hong SY, Lim JOJ (2006) The WRF single-moment 6-class microphysics scheme. J Korean Meteorol Soc 42(2):129–151

Hong SY, Noh Y, Dudhia J (2006) A new vertical diffusion package with an explicit treatment of entrainment processes. Mon Weather Rev 134(9):2318–2341

Hong SY, Lim KSS, Kim JH, Lim JOJ, Dudhia J (2009) Sensitivity study of cloud-resolving convective simulations with WRF using two bulk microphysical parameterizations: Ice-phase microphysics versus sedimentation effects. J Appl Meteorol Climatol 48(1):61–76

Huang WR, Chan JCL (2014) Dynamical downscaling forecasts of Western North Pacific tropical cyclone genesis and landfall. Clim Dyn 42(7):2227–2237

Huang WR, Chan JCL, Au-Yeung AYM (2013) Regional climate simulations of summer diurnal rainfall variations over East Asia and Southeast China. Clim Dyn 40(7):1625–1642

Jin CS, Ho CH, Kim JH, Lee DK, Cha DH, Yeh SW (2012) Critical role of northern off-equatorial sea surface temperature forcing associated with Central Pacific El Niño in more frequent tropical cyclone movements toward East Asia. J Clim 26(8):2534–2545

Jin H, Peng MS, Jin Y, Doyle JD (2014) An evaluation of the impact of horizontal resolution on tropical cyclone predictions using COAMPS-TC. Weather Forecast 29(2):252–270

Kain JS (2004) The Kain–Fritsch convective parameterization: an update. J Appl Meteorol 43(1):170–181

Kiehl JT, Hack JJ, Bonan GB, Boville BA, Briegleb BP, Williamson DL, Rasch PJ (1996) Description of the NCAR Community Climate Model (CCM3). Technical Note TN-420+STR, National Center for Atmospheric Research, Boulder, Colorado (United States). https://opensky.ucar.edu/islandora/object/technotes:187/datastream/PDF/view. Accessed 15 July 2016

Knutson TR, Sirutis JJ, Garner ST, Held IM, Tuleya RE (2007) Simulation of the recent multidecadal increase of Atlantic hurricane activity using an 18-km-grid regional model. Bull Am Meteorol Soc 88(10):1549–1565

Knutson TR, McBride JL, Chan JCL, Emanuel KA, Holland GJ, Landsea C, Held IM, Kossin JP, Srivastava AK, Sugi M (2010) Tropical cyclones and climate change. Nat Geosci 3(3):157–163

Lander MA (1996) Specific tropical cyclone track types and unusual tropical cyclone motions associated with a reverse-oriented monsoon trough in the Western North Pacific. Weather Forecast 11(2):170–186

Landman WA, Seth A, Camargo SJ (2005) The effect of regional climate model domain choice on the simulation of tropical cyclone-like vortices in the Southwestern Indian Ocean. J Clim 18(8):1263–1274

Liu KS, Chan JCL (2017) Variations in the power dissipation index in the East Asia Region. Clim Dyn 48(5):1963–1985

Mlawer EJ, Taubman SJ, Brown PD, Iacono MJ, Clough SA (1997) Radiative transfer for inhomogeneous atmospheres: RRTM, a validated correlated-k model for the longwave. J Geophys Res 102(D14):16,663–16,682

Monin A, Obukhov A (1954) Basic laws of turbulent mixing in the surface layer of the atmosphere. Trudy Geofizicheskogo Instituta Akademiya Nauk SSSR 24(151):163–187

Pal JS, Small EE, Eltahir EAB (2000) Simulation of regional-scale water and energy budgets: representation of subgrid cloud and precipitation processes within RegCM. J Geophys Res 105(D24):29,579–29,594

Pal JS, Giorgi F, Bi X, Elguindi N, Solmon F, Rauscher SA, Gao X, Francisco R, Zakey A, Winter J, Ashfaq M, Syed FS, Sloan LC, Bell JL, Diffenbaugh NS, Karmacharya J, Konaré A, Martinez D, da Rocha RP, Steiner AL (2007) Regional climate modeling for the developing world: the ICTP RegCM3 and RegCNET. Bull Am Meteorol Soc 88(9):1395–1409

Parker CL, Lynch AH, Arbetter TE (2013) Evaluating WRF-ARW v3.4.1 simulations of Tropical Cyclone Yasi. In: 14th annual WRF Users' Workshop, National Center for Atmospheric Research, Boulder (United States). http://www2.mmm.ucar.edu/wrf/users/workshops/WS2013/extended_abstracts/7B.6.pdf. Accessed 15 July 2016

Qian YK, Liang CX, Yuan Z, Peng S, Wu J, Wang S (2016) Upper-tropospheric environment-tropical cyclone interactions over the western North Pacific: a statistical study. Adv Atmos Sci 33(5):614–631

Saha S, Moorthi S, Pan HL, Wu X, Wang J, Nadiga S, Tripp P, Kistler R, Woollen J, Behringer D, Liu H, Stokes D, Grumbine R, Gayno G, Wang J, Hou YT, Chuang HY, Juang HMH, Sela J, Iredell M, Treadon R, Kleist D, van Delst P, Keyser D, Derber J, Ek M, Meng J, Wei H, Yang R, Lord S, van den Dool H, Kumar A, Wang W, Long C, Chelliah M, Xue Y, Huang B, Schemm JK, Ebisuzaki W, Lin R, Xie P, Chen M, Zhou S, Higgins W, Zou CZ, Liu Q, Chen Y, Han Y, Cucurull L, Reynolds RW, Rutledge G, Goldberg M (2010) The NCEP climate forecast system reanalysis. Bull Am Meteorol Soc 91(8):1015–1057

Saha S, Moorthi S, Wu X, Wang J, Nadiga S, Tripp P, Behringer D, Hou YT, Hy Chuang, Iredell M, Ek M, Meng J, Yang R, Mendez MP, van den Dool H, Zhang Q, Wang W, Chen M, Becker E (2014) The ncep climate forecast system version 2. J Clim 27(6):2185–2208

Skamarock WC, Klemp JB, Dudhia J, Gill DO, Barker DM, Duda MG, Huang XY, Wang W, Powers JGa (2008) A description of the advanced research WRF version 3. Technical Note TN-475+STR, National Center for Atmospheric Research, Boulder, Colorado (United States). https://opensky.ucar.edu/islandora/object/technotes:500/datastream/PDF/view. Accessed 15 July 2016

Stowasser M, Wang Y, Hamilton K (2007) Tropical cyclone changes in the Western North Pacific in a global warming scenario. J Clim 20(11):2378–2396

Tiedtke M (1989) A comprehensive mass flux scheme for cumulus parameterization in large-scale models. Mon Weather Rev 117(8):1779–1800

Uppala SM, KÅllberg PW, Simmons AJ, Andrae U, Bechtold VDC, Fiorino M, Gibson JK, Haseler J, Hernandez A, Kelly GA, Li X, Onogi K, Saarinen S, Sokka N, Allan RP, Andersson E, Arpe K, Balmaseda MA, Beljaars ACM, Berg LVD, Bidlot J, Bormann N, Caires S, Chevallier F, Dethof A, Dragosavac M, Fisher M, Fuentes M, Hagemann S, Hólm E, Hoskins BJ, Isaksen L, Janssen PAEM, Jenne R, Mcnally AP, Mahfouf JF, Morcrette JJ, Rayner NA, Saunders RW, Simon P, Sterl A, Trenberth KE, Untch A, Vasiljevic D, Viterbo P, Woollen J (2005) The ERA-40 re-analysis. Q J R Meteorol Soc 131(612):2961–3012

Vitart F, Stockdale TN (2001) Seasonal forecasting of tropical storms using coupled GCM integrations. Mon Weather Rev 129(10):2521–2537

Wang B, Chan JCL (2002) How strong ENSO events affect tropical storm activity over the Western North Pacific. J Clim 15(13):1643–1658

Wang C, Wu L (2016) Interannual shift of the tropical upper-tropospheric trough and its influence on tropical cyclone formation over the western North Pacific. J Clim 29(11):4203–4211

Watterson IG, Evans JL, Ryan BF (1995) Seasonal and interannual variability of tropical cyclogenesis: diagnostics from large-scale fields. J Clim 8(12):3052–3066